



AFRL-AFOSR-JP-TR-2017-0007

Investigation of Chirality Selection Mechanism of Single-Walled Carbon Nanotube

Seun Min Kim
KOREA INSTITUTE OF SCIENCE AND TECHNOLOGY (KIST)

12/13/2016
Final Report

DISTRIBUTION A: Distribution approved for public release.

Air Force Research Laboratory
AF Office Of Scientific Research (AFOSR)/ IOA
Arlington, Virginia 22203
Air Force Materiel Command

REPORT DOCUMENTATION PAGE					Form Approved OMB No. 0704-0188	
<p>The public reporting burden for this collection of information is estimated to average 1 hour per response, including the time for reviewing instructions, searching existing data sources, gathering and maintaining the data needed, and completing and reviewing the collection of information. Send comments regarding this burden estimate or any other aspect of this collection of information, including suggestions for reducing the burden, to Department of Defense, Executive Services, Directorate (0704-0188). Respondents should be aware that notwithstanding any other provision of law, no person shall be subject to any penalty for failing to comply with a collection of information if it does not display a currently valid OMB control number.</p> <p>PLEASE DO NOT RETURN YOUR FORM TO THE ABOVE ORGANIZATION.</p>						
1. REPORT DATE (DD-MM-YYYY) 19-01-2017		2. REPORT TYPE Final		3. DATES COVERED (From - To) 18 Sep 2015 to 17 Sep 2016		
4. TITLE AND SUBTITLE Investigation of Chirality Selection Mechanism of Single-Walled Carbon Nanotube				5a. CONTRACT NUMBER		
				5b. GRANT NUMBER FA2386-15-1-4099		
				5c. PROGRAM ELEMENT NUMBER 61102F		
6. AUTHOR(S) Seun Min Kim				5d. PROJECT NUMBER		
				5e. TASK NUMBER		
				5f. WORK UNIT NUMBER		
7. PERFORMING ORGANIZATION NAME(S) AND ADDRESS(ES) KOREA INSTITUTE OF SCIENCE AND TECHNOLOGY (KIST) 39-1 HAWEOLGOK-DONG, SUNGBUK-KU SEOUL, 136-791 KR				8. PERFORMING ORGANIZATION REPORT NUMBER		
9. SPONSORING/MONITORING AGENCY NAME(S) AND ADDRESS(ES) AOARD UNIT 45002 APO AP 96338-5002				10. SPONSOR/MONITOR'S ACRONYM(S) AFRL/AFOSR IOA		
				11. SPONSOR/MONITOR'S REPORT NUMBER(S) AFRL-AFOSR-JP-TR-2017-0007		
12. DISTRIBUTION/AVAILABILITY STATEMENT A DISTRIBUTION UNLIMITED: PB Public Release						
13. SUPPLEMENTARY NOTES						
14. ABSTRACT <p>This research involved investigation of two fundamental mechanisms of carbon nanotube (CNT) growth: chirality selection of single-walled CNT (SWCNT) and growth improvement of CNT arrays. For the chirality selection mechanism, attempts to use thin membrane TEM samples to clearly observe CNT/catalyst particle interfaces under optimized growth conditions was unsuccessful. Instead, in-situ CNT growth array experiments on rational design of catalyst layers using TEM holders showed significant advancement. This involved investigation of the effects of sub-supporting SiO₂ layer on the interaction between Fe particles and supporting Al₂O₃ layer for uniform and stable growth of CNT forests. The results show that catalyst particles with a higher number density are formed on the Al₂O₃ layer deposited on the sub-supporting SiO₂ layer than that deposited directly on the Si(100) wafer. Based on the cross-sectional TEM images, liquid contact angle measurements, and ellipsometry analyses, the Al₂O₃ layer deposited on thermally grown SiO₂ layer is found to have a lower porosity, resulting in a lower adhesion (higher wetting angle) between Fe and Al₂O₃. In addition, the sub-supporting SiO₂ layer acts as a diffusion barrier to prevent the formation of a new phase with Si crystal. These factors help in maintaining a high number density of Fe catalyst particles. Therefore, in order to grow CNT forests with a high population density, it is desirable to use the SiO₂ sub-supporting layer under the Al₂O₃ layer. In addition, in order to maintain the catalyst size and number distribution during CNT growth, a new catalyst preparation method has been developed via an Fe ion is implantation method.</p>						
15. SUBJECT TERMS Carbon Nanotubes, Catalysis, Chirality, Processing, Mechanism						
16. SECURITY CLASSIFICATION OF:			17. LIMITATION OF ABSTRACT SAR	18. NUMBER OF PAGES 22	19a. NAME OF RESPONSIBLE PERSON CASTER, KENNETH	
a. REPORT Unclassified	b. ABSTRACT Unclassified	c. THIS PAGE Unclassified			19b. TELEPHONE NUMBER (Include area code) 315-229-3326	

Final Report for AOARD Grant FA2386-15-1-4099

“Investigation of chirality selection mechanism of single-walled carbon nanotube”

Date: 12/13/2016

PI and Co-PI information:

- Name of Principal Investigator: Seung Min Kim
- E-mail address: seungmin.kim@kist.re.kr
- Institution: Korea Institute of Science and Technology
- Department: Carbon Composite Materials Research Center
- Mailing Address: Chudong-ro 92, Bongdong-eup, Wanju-gun, Jeonbuk 55324, South Korea
- Phone: +82-63-219-8154
- Fax: +82-63-219-8419

Period of Performance: 9/18/2015 ~ 9/17/2016

Abstract:

In the second year of the project, we have investigated two fundamental mechanisms of carbon nanotube (CNT) growth: chirality selection of single-walled CNT (SWCNT) and growth improvement of CNT arrays based on the results in the first year of the project. For the chirality selection mechanism, we have tried to optimize growth conditions using the thin membrane TEM sample for clearly observing the interfaces between CNTs and catalyst particles. However, the approach was not quite successful. Instead, we initiated to perform in-situ CNT growth experiments using in-situ TEM holders, which were installed at KIST in August of 2016. For the growth improvement of CNT arrays by rational design of catalyst layers, we have made a significant advancement for the last two years. Especially in the second year of the project, we have investigated the effects of sub-supporting SiO₂ layer on the interaction between Fe particles and supporting Al₂O₃ layer for uniform and stable growth of CNT forests. Our results show that catalyst particles with a higher number density are formed on the Al₂O₃ layer deposited on the sub-supporting SiO₂ layer than that deposited directly on the Si(100) wafer. Based on the cross-sectional TEM images, liquid contact angle measurements, and ellipsometry analyses, the Al₂O₃ layer deposited on thermally grown SiO₂ layer is found to have a lower porosity, resulting in a lower adhesion (higher wetting angle) between Fe and Al₂O₃. In addition, the sub-supporting SiO₂ layer acts as a diffusion barrier to prevent the formation of a new phase with Si crystal. These factors help in maintaining a high number density of Fe catalyst particles on the Fe 1

nm/ Al_2O_3 10 nm/ SiO_2 300 nm/ $\text{Si}(100)$ sample. Therefore, in order to grow CNT forests with a high population density, it is desirable to use the SiO_2 sub-supporting layer under the Al_2O_3 layer. In addition, in order to maintain the catalyst size and number distribution during CNT growth, a new catalyst preparation method has been developed: Fe ion implantation method. When the Fe implanted SiO_2/Si wafer is annealed, Fe particles diffuse out to the surface of the wafer. The distribution of these particles is uniformly maintained even after 12 h of annealing in Ar ambient. Thus, the Fe particles formed from Fe-implanted SiO_2/Si wafer are expected to produce uniform and long CNT forests.

Introduction:

In the second year of the project, we have performed the research into two directions following the plan suggested in the second-year proposal: (1) the investigation of the chirality selection mechanism and (2) the improvement of carbon nanotube (CNT) array growth by the rational design of the catalyst layer for suppressing the processes leading to CNT growth termination. In order to investigate chirality selection mechanisms of single-walled CNTs (SWCNTs), we tried to optimize SWCNT growth conditions, where less dense, very short, and highly crystalline SWCNTs can be synthesized. In that way, we expected that we could obtain enough statistics to clearly observe the interfaces between SWCNTs and metallic catalysts based on the focused ion beam (FIB) based transmission electron microscopy (TEM) sample preparation method, which we developed in the first year of the project. However, we could not successfully find proper growth conditions. In addition, we realized, even though we could observe the interfaces by ex-situ experiments, the structural correlation between SWCNTs and metallic catalysts needs to be confirmed by in-situ experiments. Therefore, we changed a strategy for performing in-situ experiments using in-situ TEM holders, which were installed at KIST in August of 2016.

For the improvement of CNT array growth by suppressing the processes leading to CNT growth termination, we have made big advances. The evolution in catalyst morphology causes the growth termination. Thus, the maintenance of catalyst particles is the key to the growth of long CNTs. In the first year of the project, in order to minimize the evolution of catalyst morphology, we have emphasized the importance of the interaction between catalyst and supporting layer. As supporting layer for metallic catalyst particles, Al_2O_3 layer has been shown to possess superior ability to support vertically aligned growth of CNTs [1]. The role of Al_2O_3

layer has been studied with respect to various aspects. The suggested roles of Al_2O_3 layer are to maintain strong interaction between Fe and Al_2O_3 layer to minimize surface migration of particles [2], to enhance catalytic activity of catalysts to reform hydrocarbons [3, 4], to prevent the metallic catalysts from forming metal silicides [5], and to change the chemical state of supported catalysts [6]. The type of alumina used can also affect the growth of CNT forests owing to the differences in the surface properties [1, 7].

However, only a few studies have reported on the role of the sub-supporting layer in the growth of CNT forests. This is due to a common belief that the sub-supporting layer would not significantly affect the formation of catalysts while the supporting layer does affect. In our experience of growing CNT forest, however, we observed that the presence of sub-supporting layer does affect the growth of CNT forests. In particular, the presence of the sub-supporting layer such as thermally grown SiO_2 layer makes clear difference in terms of the alignment of CNT forests. However, there has been no clear statement or fundamental research so far that a SiO_2 sub-supporting layer plays a crucial role in the growth of CNT forest.

To the best of our knowledge, only one study has reported the effects of the sub-supporting layer on the growth of CNT forests [8]. In their work, the thickness and morphology of the catalyst sub-supporting SiO_2 layer were varied. The morphology differences of the SiO_2 sub-supporting layer affected the size and number density of the Fe catalyst particles and the growth of CNT forests [8]. However, the effects of the presence of a SiO_2 sub-supporting layer on the CNT forest growth have not yet been investigated. Understanding the role of SiO_2 sub-supporting layer on the growth of CNT forests is critical for achieving highly controllable growth of CNT forests.

In the second year, we investigated the effects of a SiO_2 sub-supporting layer by comparing Si(100) wafers with only native SiO_2 and thermally grown 300-nm-thick SiO_2 layers. We employed atomic force microscopy (AFM), the transmission electron microscopy (TEM), and ellipsometry techniques for examining the different morphological evolutions of catalyst particles and Al_2O_3 support layer on two substrates, which would lead to the difference in the growth of CNT forests.

In addition, we have developed a new method to prepare catalysts for the growth of CNT forests using Fe ion implantation technique. The morphology of Fe catalyst particles by Fe ion implantation followed by annealing for 15 minutes in Ar ambient rarely evolves up to 12 hours annealing. This means that this new method has a potential to form very stable Fe particles

during the CNT growth and lead to extremely long CNT growth, even though further studies to thoroughly understand catalyst forming processes and subsequent CNT growth are absolutely necessary.

Experiment:

- Growth of CNT forests on Fe deposited substrates with and without sub-supporting SiO₂ layer

Two types of substrates, silicon (100) wafer and silicon (100) wafer with a 300-nm-thick SiO₂ layer, were used in this study. The substrates were first coated with a 10-nm-thick Al₂O₃ layer by atomic layer deposition (ALD) followed by coating with a 1-nm-thick Fe thin film by e-beam evaporation. The substrates were cut into small pieces in the dimensions of about 1 cm × 1 cm for performing annealing and growth experiments.

An atmospheric CVD technique using a Lindberg Blue M (HTF55322) tube furnace was used for the growth of spinnable CNT forests. Catalyst-coated substrates were loaded into the middle of a quartz tube having an inner diameter of 38 mm and a length of 700 mm. The temperature was ramped to 670 °C in 20 min under an Ar flow of 400 standard cubic centimeters per minute (sccm). Then, a gas mixture of C₂H₂ (19 sccm), H₂ (95 sccm), and Ar (286 sccm) was fed for 3-10 min for growing the CNT forest. The heater was turned off after the growth, and the substrates were removed after cooling down the reactor below 100 °C under Ar gas flow.

- Annealing of catalyst-coated substrates

Annealing of the catalyst-coated substrates was performed using the same tube furnace used in the CNT forest growth. The temperature was ramped to the target temperature in 25 min under Ar atmosphere, and the temperature was maintained under Ar or Ar/H₂ atmosphere for 10 min. The samples were removed after cooling down the furnace below 100 °C under Ar gas flow.

- Preparation of Fe ion implanted wafers

The Fe ion implanted substrate was prepared using silicon (100) wafer with a 300 nm-thick oxidized layer. Fe⁺ ion was implanted using a lab-made ion implanter at the accelerating voltage of 60 keV at Korea Multi-Purpose Accelerator Complex. The dose of Fe⁺ ion was 10¹⁶/cm². As a control sample, 1 nm-thin Fe film was deposited on a silicon (100) wafer with a 300 nm-thick oxidized layer by e-beam evaporation. For annealing, a quartz tube furnace (Lindberg/Blue M, HTF55322C, inner diameter 35 mm) was used. The Fe implanted and deposited samples were

heated to 800 °C in 15 minutes under Ar atmosphere, maintained for various times, and cooled down to room temperature.

Results and Discussion:

- Investigation of chirality selection mechanism of single-walled carbon nanotube

In order to clearly observe the interfaces between CNTs and metallic catalysts, we have optimized SWCNT growth conditions, where less dense, very short, and highly crystalline SWCNTs can be synthesized. As shown in Figure 1, in few cases, we could obtain high resolution TEM images of the interfaces between CNTs and catalyst particles using thin membrane samples, but we could not get statistically meaningful data so far. In addition, even though we could get enough data by ex-situ experiments, the structural correlation between CNTs and catalyst particles needs to be confirmed by in-situ experiments. Therefore, we decided to perform in-situ CNT growth experiments using in-situ TEM holders, which were installed at KIST in August of 2016. During initial in-situ growth experiment, we could successfully synthesize and observe carbon nanostructures as shown in Figure 2. In the third year of the project, we will continue to do in-situ experiments for investigation of chirality selection mechanisms.

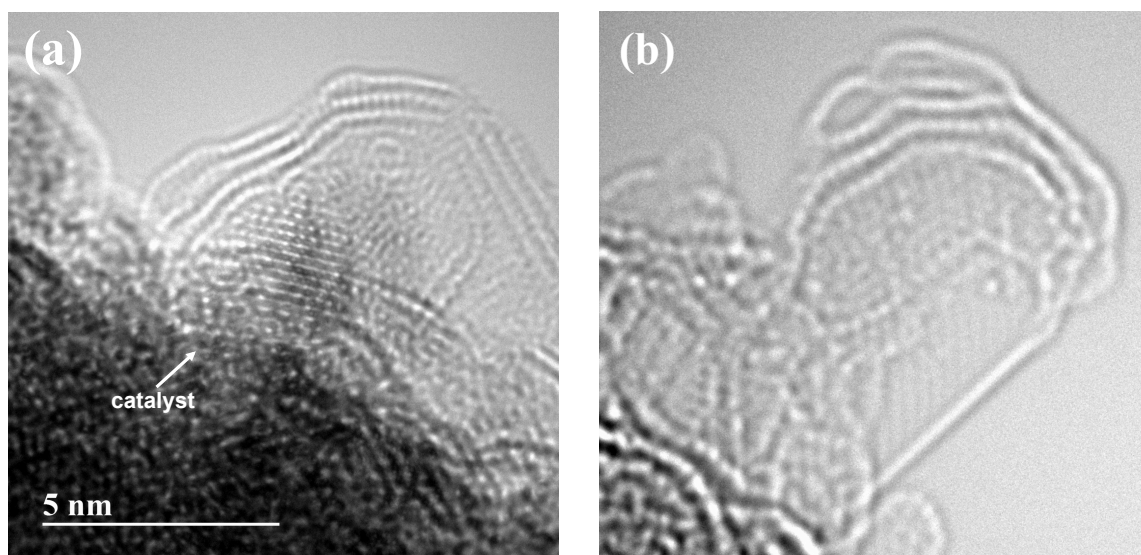


Figure 1. (a-b) High resolution TEM images of the interfaces between CNTs and catalyst particles for the investigation of chirality selection mechanisms.

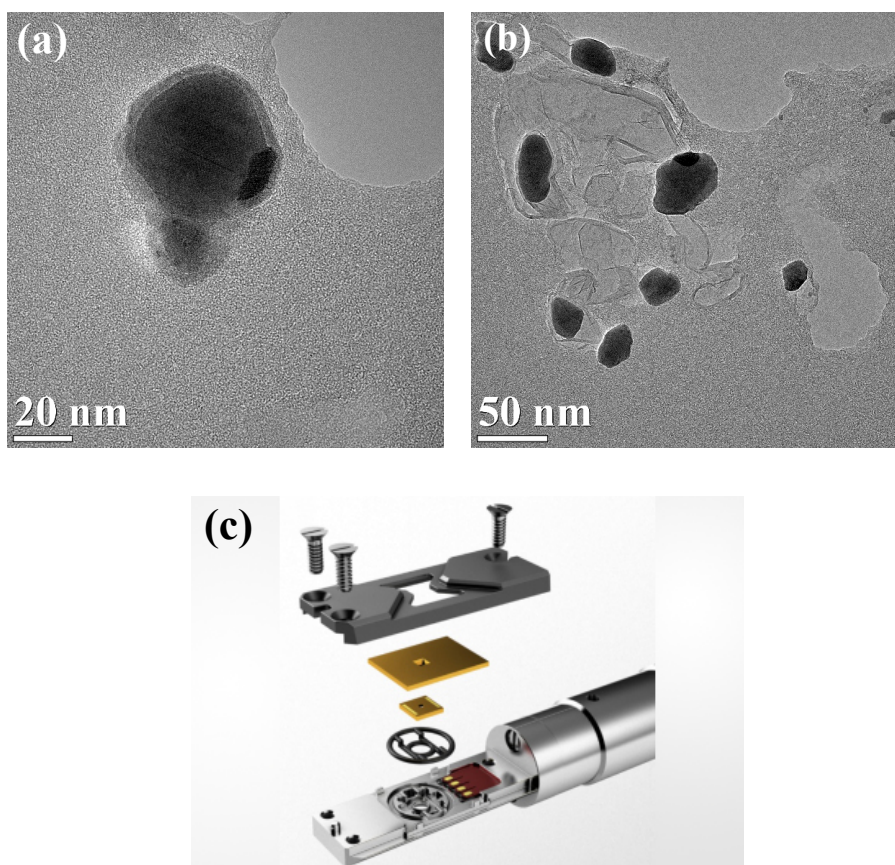


Figure 2. TEM images of (a) a catalyst particle before in-situ growth and (b) catalyst particles and carbon nanostructures during in-situ growth. (c) The schematic of in-situ TEM holder.

- Effects of SiO₂ sub-supporting layer on the growth of carbon nanotube forests

In the first year of the project, we have developed the modified growth termination model in Figure 3. In this model, the strong interaction between catalyst particles and supporting layers is of critical importance to the lifetime of catalyst particles and thus the final lengths of CNT arrays. So far, Al₂O₃ supporting layers are well known to have strong interaction with Fe catalyst particles, but the effects of sub-supporting layers on the interaction between Fe catalyst particles and Al₂O₃ supporting layers have not been yet investigated.

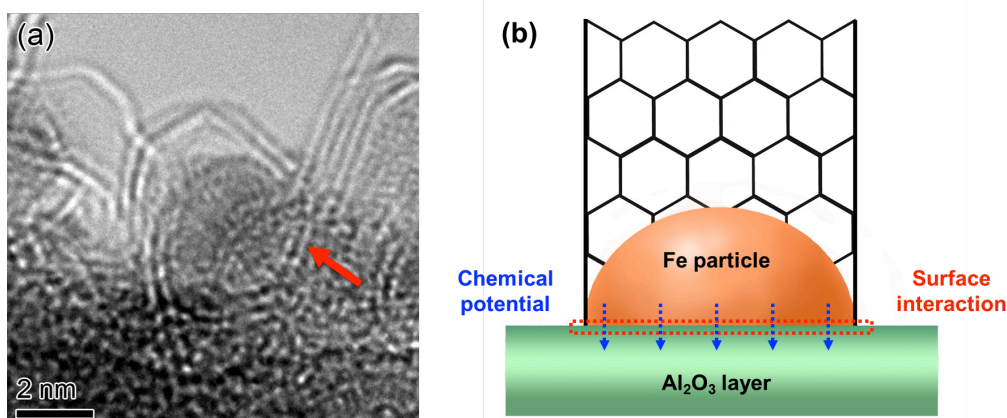


Figure 3. (a) High resolution TEM image of the catalyst particle, which nucleates and just starts to grow the CNT. The graphitic layers seem to cover the whole catalyst particle. (b) The schematic representation of a Fe particle on Al₂O₃ layer and two competing forces exerted on the Fe particle.

In order to compare the morphologies of the catalyst particles formed on the two different substrates with and without SiO₂ sub-supporting layer, the substrates were annealed under hydrogen atmosphere at various temperatures. In both the cases, it was commonly observed that larger catalyst particles are formed with an increase in the annealing temperature. Noticeable differences can be observed between the two substrates. In the presence of the SiO₂ sub-supporting layer, catalyst particles with a higher population density are formed at all temperatures ranging from 600 °C to 900 °C as compared with that prepared in the absence of SiO₂ sub-supporting layer. Especially, the catalyst particles are rarely observed at 600 °C and 700 °C on the substrates having no SiO₂ sub-supporting layer (Figures 4(a) and (b)). The roughness values of the samples shown in Figures 4(a) and (b) are 0.276 nm and 0.310 nm, respectively, and that of the as-deposited sample is 0.142 nm. This indicates that the deposited Fe layer is not completely transformed to form Fe islands on the Fe 1 nm/Al₂O₃ 10 nm/Si(100) substrates on annealing up to a temperature of 700 °C.

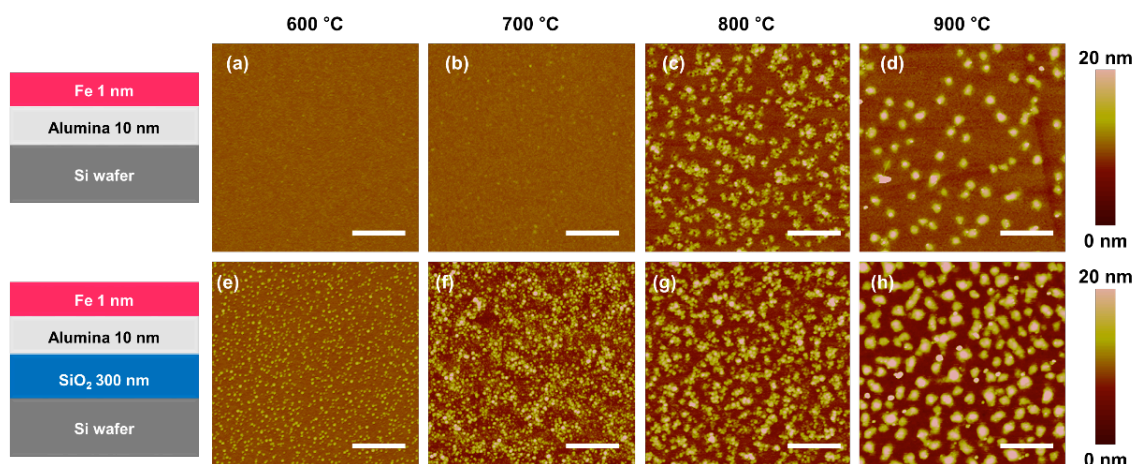


Figure 4. AFM images of the samples after subjecting to heat treatment under Ar/H₂ atmosphere for 10 min: Fe 1 nm/Al₂O₃ 10 nm/Si substrate treated at (a) 600 °C, (b) 700 °C, (c) 800 °C, and (d) 900 °C and Fe 1 nm/Al₂O₃ 10 nm/SiO₂ 300 nm/Si substrate treated at (e) 600 °C, (f) 700 °C, (g) 800 °C, (h) 900 °C. All the scale bars are 500 nm.

For a more precise examination of the catalyst particle formation, the annealed substrates were analyzed by TEM. Figure 5 shows plane-view TEM images of the two types of substrates that are annealed at 700 °C and 900 °C under H₂ atmosphere for 10 min. A clear difference in the particle number density can be observed on the two substrates. More Fe particles are formed in the presence of SiO₂ sub-supporting layer at both the temperatures examined, which is in good agreement with the AFM results. Straight and perpendicular dark lines are observed on the Fe 1 nm/Al₂O₃ 10 nm/Si substrates annealed at 700 °C and 900 °C (Figures 5(a) and (c)). Further analysis and related discussion will be dealt with later in the manuscript.

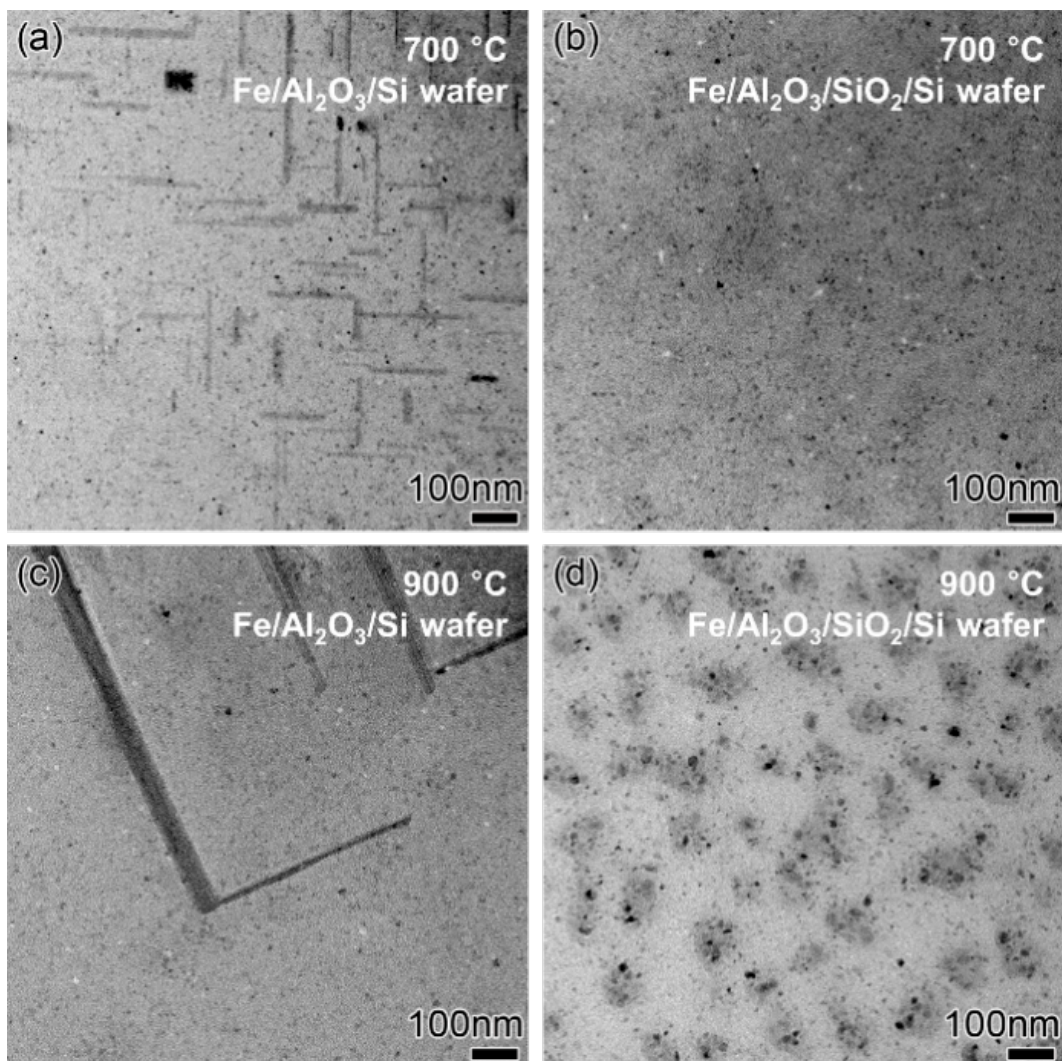


Figure 5. Plane-view TEM images of Fe 1 nm/Al₂O₃ 10 nm/Si wafer after heat treatment at (a) 700 °C and (c) 900 °C under H₂ atmosphere for 10 min and Fe 1 nm/Al₂O₃ 10 nm/SiO₂ 300 nm/Si wafer after heat treatment at (b) 700 °C and (d) 900 °C under H₂ atmosphere for 10 min.

Figure 6 shows cross-sectional TEM images of the two substrates after subjecting to annealing at 700 °C for 10 min. The surface morphology of the annealed Fe 1 nm/Al₂O₃ 10 nm/SiO₂ 300 nm/Si(100) sample shown in Figure 6(b) appears much rougher than that of annealed Fe 1 nm/Al₂O₃ 10 nm/Si(100) sample shown in Figure 6(a). This observation is also in consistence with the AFM results, by which the roughness values of the samples with and without SiO₂ sub-supporting layers are found to be 1.35 nm and 0.310 nm, respectively. Crystalline structures of Fe particles can be clearly distinguished on the amorphous Al₂O₃ layer from the corresponding high magnification TEM images (Figures 6(c) and (d)). Depending on the

presence of the sub-supporting layer, the contact angles between the Fe surface and the Al_2O_3 layer are different in the samples shown in Figures 6(c) and (d). The differences in the wetting angle of Fe catalyst particles on the Al_2O_3 supporting layer could be attributed to the differences in the surface properties of the Al_2O_3 layers. The adhesion between Fe and Al_2O_3 is stronger on Si(100) than on thermally grown SiO_2 , and thus the contact angle is lower in the former case than in the latter case. Therefore, the differences in the surface properties of Al_2O_3 layer induced by the existence of the SiO_2 layer result in the different contact angles between Fe and the Al_2O_3 layer, thereby resulting in differences in the number density of the catalyst particles.

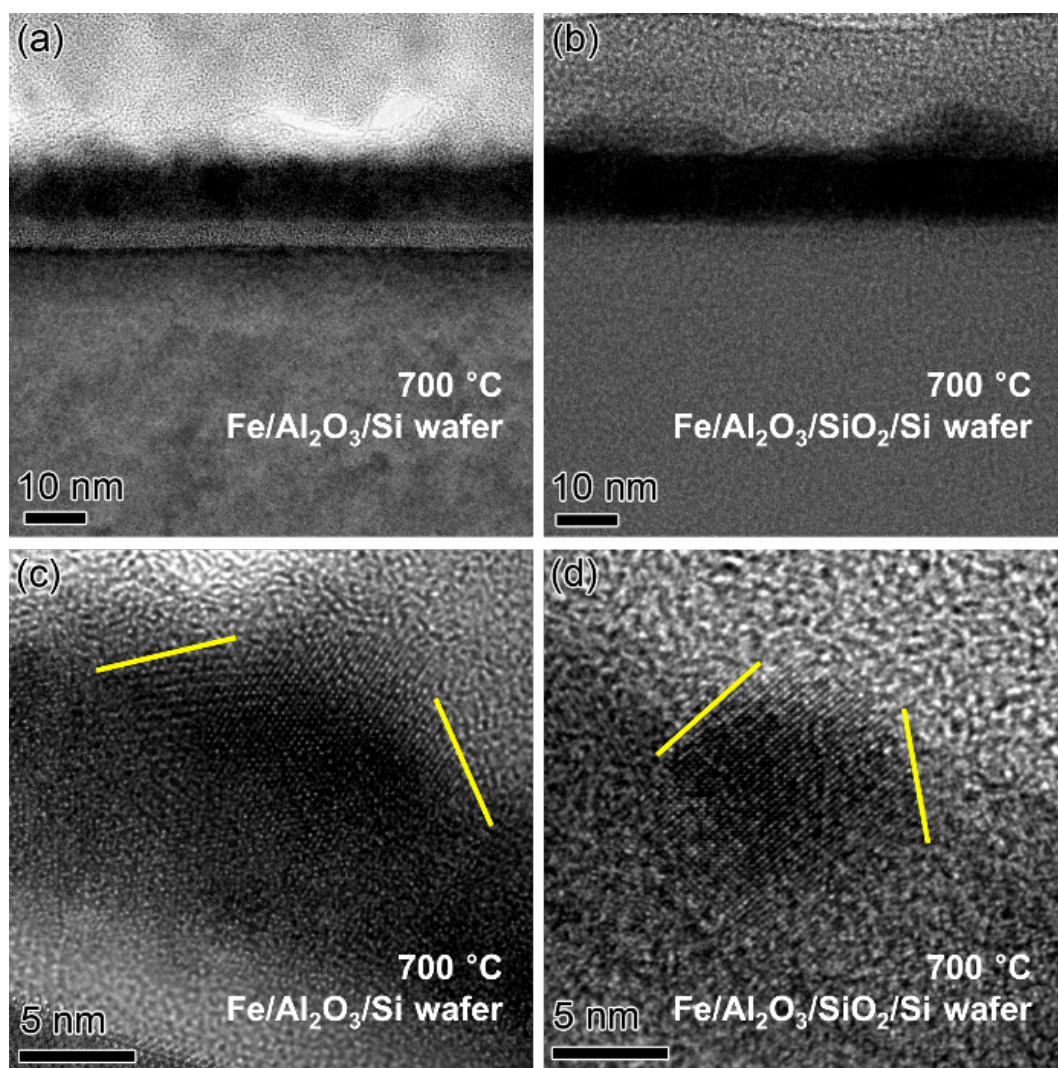


Figure 6. Cross-sectional TEM images of (a) and (c) Fe 1 nm/ Al_2O_3 10 nm/Si wafer and (b) and (d) Fe 1 nm/ Al_2O_3 10 nm/SiO₂ 300 nm/Si wafer after heat-treating at 700 °C under H_2 atmosphere for 10 min.

The cross-sectional TEM images shown in Figure 6 indicate that the surface property of Al_2O_3 layers is strongly affected by the presence of the sub-supporting SiO_2 layer. In order to further verify the effects of the sub-supporting SiO_2 layer on the surface properties of the Al_2O_3 supporting layer, we performed liquid contact angle measurements using H_2O and CH_2I_2 as the representative hydrophilic and hydrophobic liquids. For both the liquids, the contact angles are different depending on the presence of the SiO_2 sub-supporting layer as shown in Figure 7. Both substrates exhibit different contact angles with the liquids as indicated in Figure 7. Even though the interaction between Fe and Al_2O_3 is different from the H_2O - Al_2O_3 or the CH_2I_2 - Al_2O_3 interactions, the obtained results support that the surface property of the Al_2O_3 layers strongly depends on the sub-supporting layer.

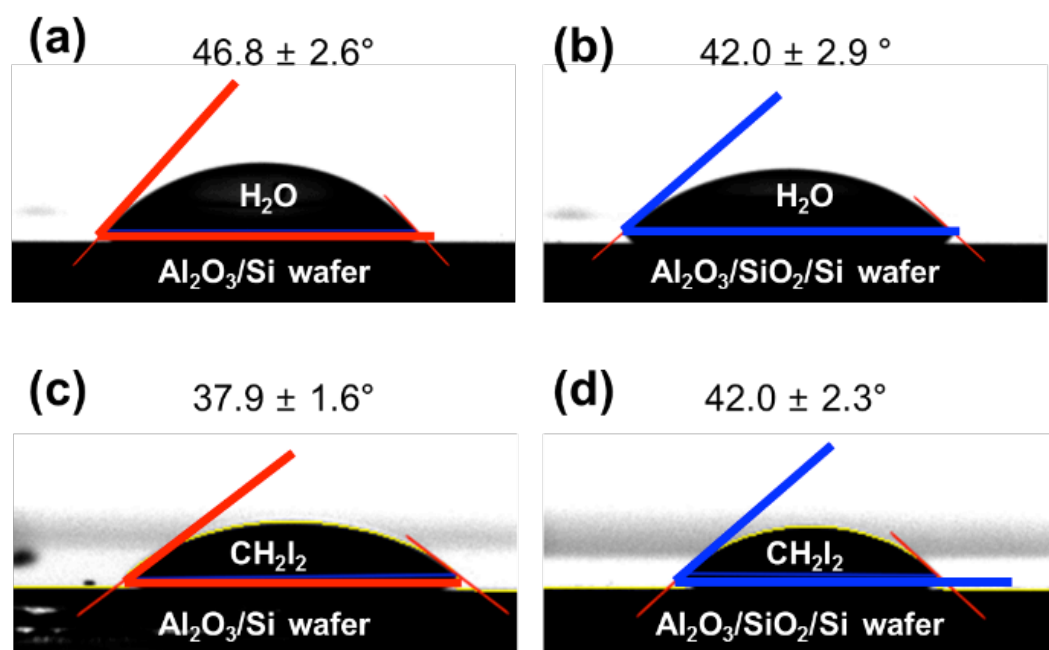


Figure 7. Images of droplets of water and diiodomethane on Al_2O_3 10 nm/Si wafer and Al_2O_3 10 nm/ SiO_2 300 nm/Si wafer indicating the variety of contact angles. A water droplet on (a) Al_2O_3 10 nm/Si wafer and (b) Al_2O_3 10 nm/ SiO_2 300 nm/Si wafer and a diiodomethane droplet on (c) Al_2O_3 10 nm/Si wafer and (d) Al_2O_3 10 nm/ SiO_2 300 nm/Si wafer.

In order to evaluate the porosity of Al_2O_3 films the ellipsometry technique was used. It is very difficult to obtain the quantitative information about the porosity of the Al_2O_3 films from

high-resolution TEM images. Assuming that the composition and thickness of Al_2O_3 films are identical, the refractive index of the Al_2O_3 films can be correlated with their porosity; porosity and refractive index have an inverse relationship [9]. Using this relationship, the ellipsometry technique has previously been used to characterize the porosity of alumina films where the influence of alumina type on the growth of CNT forest was studied [1]. In our case, the STEM-EDS analysis shows that the atomic ratios of Al to O for both Al_2O_3 films are nearly identical, and the thicknesses of the two films are also similar as observed from TEM images in Figures 6(a) and (b). Thus, we can correlate the optical properties of the Al_2O_3 films measured by ellipsometry with the porosity of the Al_2O_3 films with and without sub-supporting SiO_2 layer. Figure 8 displays the index of refraction of Al_2O_3 10 nm/Si(100) and Al_2O_3 10 nm/ SiO_2 300 nm/Si(100) substrates as a function of wavelength. Since lower refractive index indicates higher porosity [1], the Al_2O_3 film grown on the Si(100) substrate is found to have a higher porosity than that grown on the SiO_2 /Si(100) substrate. The difference in the porosity of the Al_2O_3 layers may be responsible for the different surface properties such as the oxidation state, morphology, and surface energy, which in turn results in variations in the wetting angles between Fe and Al_2O_3 layers formed on the two substrates indicated in Figure 6. The influence of the SiO_2 sub-supporting layer on the properties of the Al_2O_3 layer may result from the deposition method of Al_2O_3 . Al_2O_3 supporting layer was deposited using a layer-by-layer deposition process by ALD which would affect the structure of the first Al_2O_3 layer depending on the surface state of the underlying substrates. This should also result in different structures of the subsequent Al_2O_3 layers, leading to the difference in the porosity.

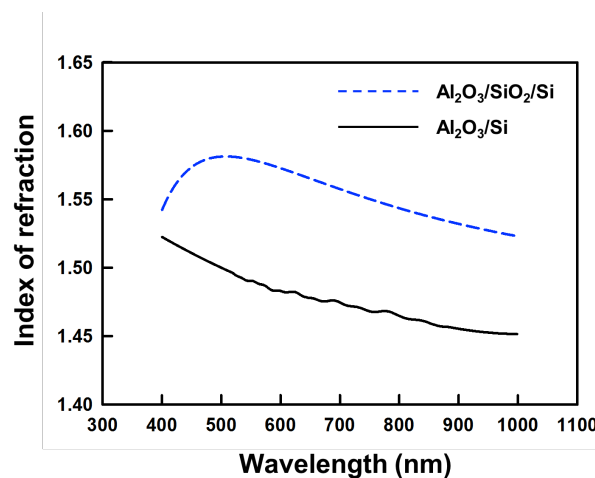


Figure 8. Index of refraction as a function of wavelength for as-deposited Al_2O_3 10 nm/ SiO_2 300

nm/Si wafer (dashed line) and Al₂O₃ 10 nm/Si wafer (solid line).

Based on the ellipsometry results shown in Figure 8, the Al₂O₃ supporting layers on Si(100) and on SiO₂/Si(100) seem to exhibit different porosities. The difference in porosity would cause the difference in the surface properties of Al₂O₃, which in turn would result in the difference in the contact angle between Fe and Al₂O₃ layers. Therefore, lower contact angle between Fe and Al₂O₃ on Si(100), i.e. stronger adhesion between Fe and Al₂O₃ layer, retards the formation of Fe islands. This leads to a much lower Fe particle areal density in the case of the Fe 1 nm/Al₂O₃ 10 nm/Si(100) sample.

Furthermore, the porous nature of the Al₂O₃ layer would cause Fe to diffuse into Al₂O₃ layer, as reported in previous studies [1, 7, 10]. Even though we carried out annealing of the samples only for 10 min, which usually corresponds to the reduction step before the actual growth step, the Fe elemental mapping images by EDS given in Figures 9(b) and (d) indicate that Fe is already diffused into the whole Al₂O₃ layer. For comparison, the high angle annular dark field (HAADF) scanning TEM (STEM) images are shown in Figures 9(a) and (c), respectively. As seen in Figures 9(c) and (d), a different phase nucleates from Si and grows into the Si substrate. The Fe elemental mapping in Figure 9(d) confirms that the new phase contains Fe. This Fe-containing phase corresponds to the straight lines observed in the plane-view TEM images shown in Figures 5(a) and (c). These lines are only observed when Al₂O₃ is deposited directly on the Si(100) wafer, and become larger as the temperature increases as presented in Figures 5(a) and (c). The high-resolution TEM image of the interface between Al₂O₃ and Si in Figure 9(e) indicates that the Fe-containing phase nucleates at the surface of Si and propagates into the Si crystal. Fast Fourier transform (FFT) patterns from the Si crystal and the new phase shown in the insets of Figure 9(f) are clearly distinguishable and the pattern from the new phase (inset shown at the upper right corner in Figure 9(f)) matches with that of the FeSi₂ phase [11]. However, in the case of Fe 1 nm/Al₂O₃ 10 nm/SiO₂ 300 nm/Si(100), the thermally grown sub-supporting SiO₂ layer acts as a diffusion barrier against Fe, thereby stopping the Fe diffusion as shown in the TEM images (Figures 6(b), 9(a), and 9(b)). This observation is also related to the lower number density of Fe particles on the Al₂O₃/Si(100) than on the Al₂O₃/SiO₂/Si(100), which would strongly affect the growth, and alignment of the CNT forests.

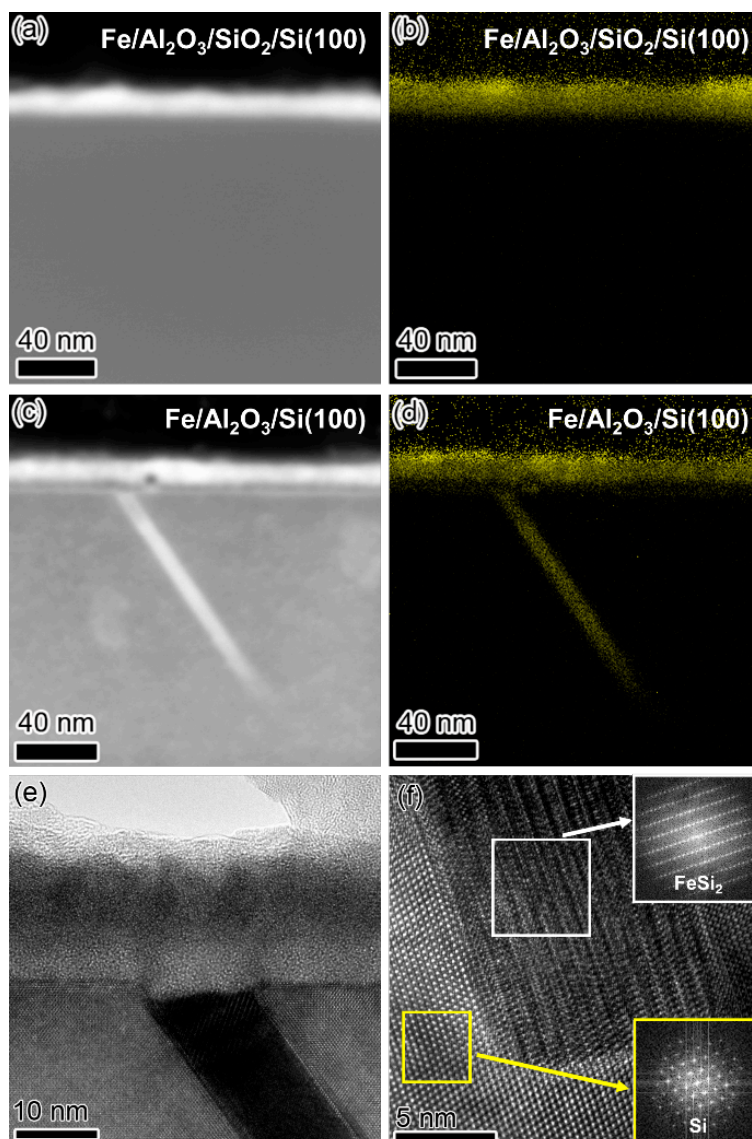


Figure 9. (a) HAADF STEM image of the cross-section of Fe 1 nm/Al₂O₃ 10 nm/SiO₂ 300 nm/Si wafer and (b) the corresponding Fe elemental mapping image. (c) HAADF STEM image of the cross-section of Fe 1 nm/Al₂O₃ 10 nm/Si wafer and (d) the corresponding Fe elemental mapping image. (e) and (f) Cross-sectional TEM images of the sample given in (c). Insets in (f) show the reduced FFT images corresponding to the marked area. All the samples were treated at 700 °C under H₂ atmosphere for 10 min.

In summary, we investigated the influence of SiO₂ sub-supporting layer present under the Al₂O₃ layer on the growth of CNT forests. The areal number density of the Fe catalyst particles shows the clear difference depending on the presence of the thermally grown SiO₂ sub-supporting layer, which critically affects the alignment of CNT forests. Catalyst particles

with a higher number density are formed on the Al_2O_3 layer deposited on the sub-supporting SiO_2 layer than that deposited directly on the $\text{Si}(100)$ wafer. Based on the cross-sectional TEM images, liquid contact angle measurements, and ellipsometry analyses, the Al_2O_3 layer deposited on thermally grown SiO_2 layer is found to have a lower porosity, resulting in a lower adhesion (higher wetting angle) between Fe and Al_2O_3 . In addition, the sub-supporting SiO_2 layer acts as a diffusion barrier to prevent the formation of a new phase with Si crystal. These factors help in maintaining a large number density of Fe catalyst particles on the Fe 1 nm/ Al_2O_3 10 nm/ SiO_2 300 nm/ $\text{Si}(100)$ sample. Therefore, in order to grow CNT forests with a high population density, it is desirable to use the SiO_2 sub-supporting layer under the Al_2O_3 layer. This study opens up new possibilities to accurately control the properties of CNT forests by the rational design of the sub-supporting layer.

- New method to prepare catalysts for CNT growth: Fe ion implantation

As a new catalyst preparation method, we have taken advantage of Fe ion implantation into a SiO_2/Si wafer. When Fe ions are implanted into a SiO_2/Si wafer, they form Fe particles inside the wafer [12, 13]. Upon annealing, the Fe particles diffuse out to the surface [14], which can be used as catalysts for the growth of CNTs.

In order to investigate how Fe atoms are distributed and diffuse upon heating, the cross section of as-implanted wafer was analyzed by TEM. Figure 10 displays the cross-sectional TEM images of Fe^+ ion implanted SiO_2/Si wafer with a dose of $10^{16}/\text{cm}^2$ tracing the depth of the wafer (b-d). Fe atoms coalesced into small Fe particles and the particles are distributed throughout the SiO_2 layer in colloidal form. The standard free energy of formation of SiO_2 is lower than those of iron oxides such as Fe_2O_3 and Fe_3O_4 [15]. The stronger reactivity between Si and O prevents Fe from forming iron oxides. Thus, it is energetically favorable for Fe atoms to form Fe colloidal particles rather than replace Si in SiO_2 , breaking Si and O bond [15].

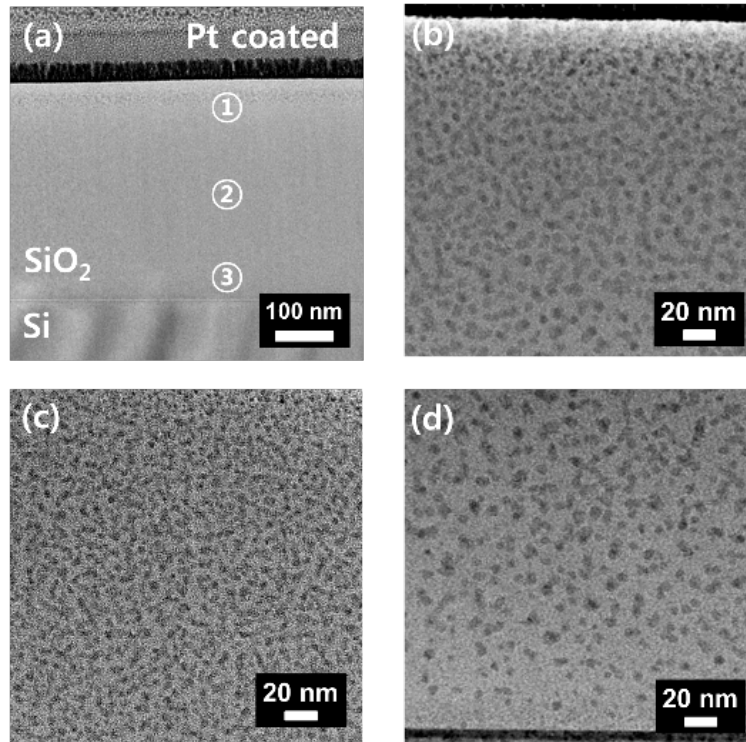


Figure 10. (a) Cross-sectional TEM image of Fe^+ ion implanted SiO_2/Si wafer with a dose of $10^{16}/\text{cm}^2$ and its higher magnification images at (b) upper, (c) middle, and (d) lower part marked as 1, 2, and 3 in (a), respectively.

The evolution of Fe particle distribution after thermal annealing was revealed by cross-sectional TEM images in Figure 11. Figure 11 shows cross-sectional TEM images of Fe^+ ion implanted SiO_2/Si wafer with a dose of $10^{16}/\text{cm}^2$ after 12 hour annealing. When the Fe implanted wafer was heated, Fe particles diffused into two directions: to the surface of the SiO_2 layer and to the SiO_2/Si interface. The number density of Fe particles in the middle of the SiO_2 layer decreased (Figure 11(c)), and the Fe particles migrated to the surface of SiO_2 layer and to the SiO_2/Si interface (Figures 11(b) and (d)).

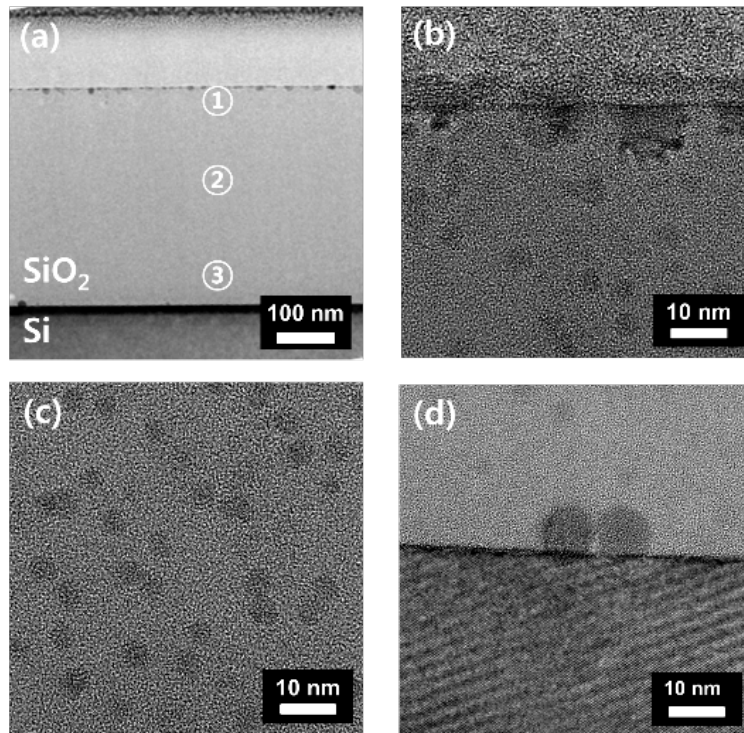


Figure 11. (a) Cross-sectional TEM image of Fe^+ ion implanted SiO_2/Si wafer with a dose of $10^{16}/\text{cm}^2$ after 12 hour annealing and its higher magnification images at (b) upper, (c) middle, and (d) lower part marked as 1, 2, and 3 in (a), respectively.

At the surface and the interface, the particles agglomerated together to form larger particles (Figures 11(b) and (d)). The larger particles at the surface of SiO_2 layer did not entirely escape to the surface, and were stuck in the SiO_2 layer, being slightly exposed to the surface. Therefore, they are reluctant to migrate, and this explains why the particle distribution of implanted wafer after thermal annealing remained nearly unchanged. This is schematically represented in Figure 12. In the as-implanted wafer, Fe ions are distributed in colloidal form following a Gaussian distribution. As they are heated, they move toward the surface of the SiO_2 layer and the interface between SiO_2 and Si, and form larger particles. The particles near the surface are stuck and tightly bound, which maintains the particle distribution nearly uniform after prolonged thermal annealing up to 12 hours.

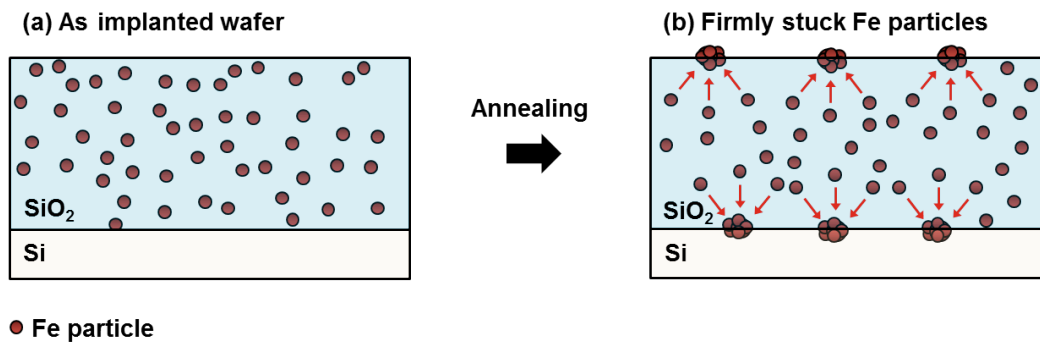


Figure 12. Schematic representation of Fe particle distribution in (a) as-implanted wafer and (b) the implanted wafer after annealing.

The distribution of Fe particles on the surface was investigated by AFM. Figure 13 shows AFM images and diameter distribution of Fe particles after various annealing times. After 15 minute annealing, Fe particles are diffused out to the surface. The diameter of particles follows a Gaussian distribution and the diameter was maintained after prolonged annealing time. Thus, this AFM result shows that the Fe ion implantation for preparation of Fe catalyst particles have great potential to produce CNT forests for a very long growth time, which is desirable for the growth of extremely long CNT forests.

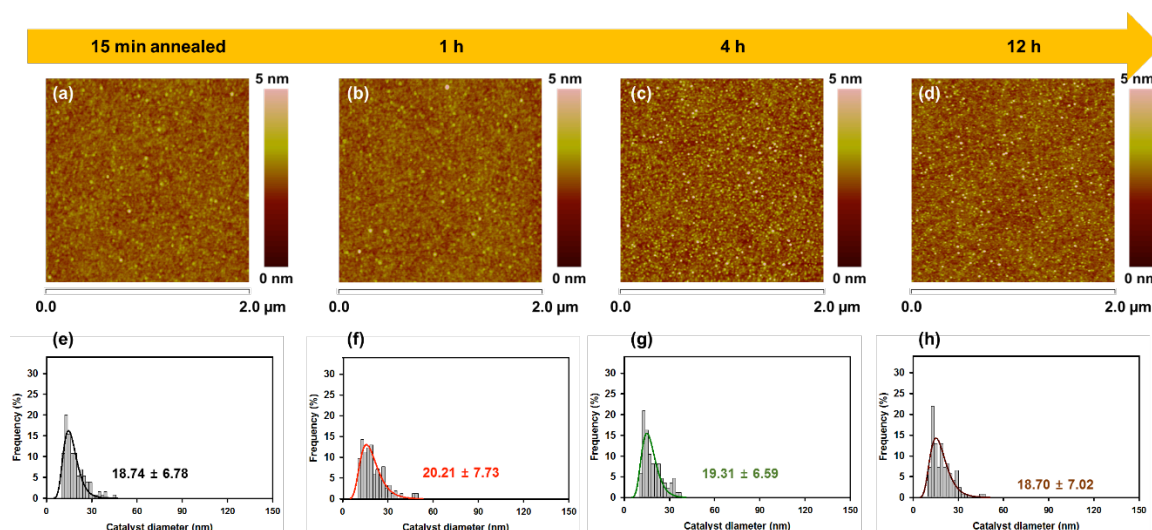


Figure 13. Change of Fe particle size after annealing at 800 °C. (a) – (d) AFM images of Fe-implanted wafers. (a) 15 min, (b) 1 h, (c) 4 h, and (d) 12 h annealing. (e) – (f) Particle size distribution of Fe-implanted wafers. (e) 15 min, (f) 1 h, (g) 4 h, and (h) 12 h annealing.

In summary, we have investigated a new catalyst preparation method, which prevents the formed catalyst particles on the surface of SiO₂/Si wafer from coalescing with each other or coarsening. This is a critical advantage of this ion implantation method over conventional e-beam evaporation method for extremely long CNT array growth. This work is still on going and will continue in the third year of the project.

References

- [1] Amama PB, Pint CL, Kim SM, McJilton L, Eyink KG, Stach EA. Influence of Alumina Type on the Evolution and Activity of Alumina-Supported Fe Catalysts in Single-Walled Carbon Nanotube Carpet Growth. *ACS Nano*. 2010;4(2):895-904.
- [2] Mattevi C, Wirth CT, Hofmann S, Blume R, Cantoro M, Ducati C, et al. In-situ X-ray Photoelectron Spectroscopy Study of Catalyst-Support Interactions and Growth of Carbon Nanotube Forests. *J. Phys. Chem. C*. 2008;112(32):12207-13.
- [3] Noda S, Hasegawa K, Sugime H, Kakehi K, Zhang Z, Maruyama S, et al. Millimeter-Thick Single-Walled Carbon Nanotube Forests: Hidden Role of Catalyst Support. *Jpn. J. Appl. Phys.* 2007;46(No. 17):L399-L401.
- [4] Magrez A, Smajda R, Seo JW, Horváth E, Ribič PR, Andresen JC, et al. Striking Influence of the Catalyst Support and Its Acid-Base Properties: New Insight into the Growth Mechanism of Carbon Nanotubes. *ACS Nano*. 2011;5(5):3428-37.
- [5] de los Arcos T, Vonau F, Garnier MG, Thommen V, Boyen HG, Oelhafen P, et al. Influence of Iron–Silicon Interaction on the Growth of Carbon Nanotubes Produced by Chemical Vapor Deposition. *Appl. Phys. Lett.* 2002;80(13):2383-5.
- [6] Arcos Tdl, Garnier MG, Seo JW, Oelhafen P, Thommen V, Mathys D. The Influence of Catalyst Chemical State and Morphology on Carbon Nanotube Growth. *J. Phys. Chem. B*. 2004;108:7728-34.
- [7] Amama PB, Putnam SA, Barron AR, Maruyama B. Wetting Behavior and Activity of Catalyst Supports in Carbon Nanotube Carpet Growth. *Nanoscale*. 2013;5(7):2642-6.
- [8] Han ZJ, Ostrikov K. Uniform, Dense Arrays of Vertically Aligned, Large-Diameter Single-Walled Carbon Nanotubes. *J. Am. Chem. Soc.* 2012;134(13):6018-24.
- [9] Reisse G, Weissmantel S, Keiper B, Steiger B, Johansen H, Martini T, et al. Influence of

Ion Bombardment on the Refractive Index of Laser Pulse Deposited Oxide Films. *Appl. Surf. Sci.* 1995;86:107-13.

[10] Kim SM, Pint CL, Amama PB, Zakharov DN, Hauge RH, Maruyama B, et al. Evolution in Catalyst Morphology Leads to Carbon Nanotube Growth Termination. *J. Phys. Chem. Lett.* 2010;1(6):918-22.

[11] Jung YJ, Wei B, Vajtai R, Ajayan PM, Homma Y, Prabhakaran K, et al. Mechanism of Selective Growth of Carbon Nanotubes on SiO₂/Si Patterns. *Nano Lett.* 2003;3(4):561-4.

[12] Leveneur J, Waterhouse GI, Kennedy J, Metson JB, Mitchell DR. Nucleation and Growth of Fe Nanoparticles in SiO₂: a TEM, XPS, and Fe L-edge XANES Investigation. *J. Phys. Chem. C.* 2011;115(43):20978-85.

[13] Strobel M, Heinig K-H, Möller W, Meldrum A, Zhou D, White C, et al. Ion Beam Synthesis of Gold Nanoclusters in SiO₂: Computer Simulations Versus Experiments. *Nuclear Instruments and Methods in Physics Research Section B: Beam Interactions with Materials and Atoms.* 1999;147(1):343-9.

[14] Oyoshi K. Migration of Ion-Implanted Fe in Silica Glass during Thermal Treatment. *Jpn. J. Appl. Phys.* 2002;41(10R):6145.

[15] Hosono H. Simple Criterion on Colloid Formation in SiO₂ Glasses by Ion Implantation. *Jpn. J. Appl. Phys.* 1993;32(9R):3892.

List of Publications and Significant Collaborations that resulted from your AOARD supported project:

- Seojeong Jeong, Jaegeun Lee, Hwan-Chul Kim, Jun Yeon Hwang, Bon-Cheol Ku, Dmitri N. Zakharov, Benji Maruyama, Eric A. Stach and Seung Min Kim*, “Direct Observation of Morphological Evolution of a Catalyst during Carbon Nanotube Forest Growth: New Insights into Growth and Growth Termination,” *Nanoscale*, **vol. 8**, pp. 2055-2062 (2016)
- Jaegeun Lee, Cheol Hun Lee, Junbeom Park, Dong-Myeong Lee, Kun-Hong Lee, Sae Byeok Jo, Kilwon Cho, Benji Maruyama, and Seung Min Kim*, “Effects of SiO₂ Sub-Supporting Layer on the Structure of Al₂O₃ Supporting Layer, Formation of Fe Catalyst Particles, and Growth of Carbon Nanotube Forests” *RSC Advances*, **vol. 6**, pp. 68424-68432 (2016)
- Frequent research discussions over phone or emails with Dr. Benji Maruyama at AFRL